Table of Contents

1. Experimental Section

Materials.

Anhydrous tin(II) chloride ($SnCl_2$, 98%, Acros), sodium oxalate ($Na_2C_2O_4$, 99.5%, Sigma-Aldrich), hydrochloric acid fuming (HCl, 37%, VWR International SA), potassium carbonate (K_2CO_3, 99.999%, Roth), potassium chloride (KCl, 99.999%, Roth) and potassium hydroxide (KOH, 1 mol·L^{-1} aqueous solution, Merck) were used as received without any purification. Deionized water (18 MΩ·cm) obtained from a Milli-Q integral water purification system (Merck Millipore Corporation) was used throughout all experiments.

Carbon black (Vulcan XC-72R) and carbon cloth (Fuel Cell Store) were first treated with ultrapure nitric acid (HNO_3, 65%, Merck) to remove the trace amount of metal. For the treatment of carbon black, 500 mg of carbon black was dispersed in 30 mL of nitric acid and kept at 80 °C for 12 hours. After the dspersion was cooled to room temperature, carbon black was collected by centrifugation, washed by deionized water until the supernatant after centrifugation was neutral, and finally vacuum dried at room temperature overnight. For the treatment of carbon cloths, 10 pieces of belt-shaped carbon cloths were merged in nitric acid at 80 °C for 12 hours, then rinsed with deionized water until the drop from the carbon cloth was neutral, and finally dried at 100 °C for 1 hour.

Synthetic procedures.

To synthesize SnC_2O_4/C, 120 mg of carbon black after the treatment of ultrapure nitric acid was dispersed in 10 mL of deionized water in a 50-mL flask, followed by the addition of 200 μL of HCl solution (36%). Then, 190 mg of anhydrous $SnCl_2$ was added into the flask under vigorous stirring. After 30 seconds, 10 mL of 0.2 M $Na_2C_2O_4$ solution was added into the flask and the mixture was kept under stirring at 25 °C for 30 min. The crude product was collected by centrifugation, and washed by deionized water twice, followed by vacuum drying at room temperature.

To prepare SnO/C, the as-synthesized SnC_2O_4/C was loaded in a quartz boat placed in a tube furnace with N_2 flow. To prepare SnO_2/C, SnC_2O_4/C was loaded in a corundum crucible in a muffle. In both syntheses, the sample was heated to 400 °C with a ramping rate of 5 °C·min^{-1}, kept at 400 °C for 4 hours, and finally collected after cooling to room temperature.

To prepare l-SnO/C, the amount of carbon black was increased to 600 mg in the synthesis of SnC_2O_4/C precursor.

To prepare Sn/C, 10 mL of aqueous solution containing 380 mg of $NaBH_4$ was added into 10 mL of aqueous dispersion containing 120 mg of carbon black, 20 μL of HCl and 190 mg of anhydrous $SnCl_2$, and the mixture was stirred at 25 °C for 30 min. Sn/C was collected by centrifugation, washed by deionized water twice, and dried under vacuum at room temperature.

Characterizations.

XRD patterns were collected on a X'Pert Philips diffractometer with monochromatic Cu Kα radiation and a fast Si-PIN multi-strip detector. The contribution of Cu Kα2 radiation was subtracted. The as-synthesized samples were directly used for XRD analysis.

HAADF-STEM and HRTEM images were collected on a FEI Tecnai Osiris TEM equipped with high-brightness field emission gun (XFEG). Samples for TEM were prepared by drying a drop of diluted ethanol dispersion of the samples onto a copper grid covered by ultrathin carbon membrane. More than 170 particles were measured to evaluate the average size of each sample.

XPS characterizations were performed on a PHI5000 VersaProbe II XPS system by Physical Electronics (PHI) with a detection limit of 1 at%. Monochromatic X-rays were generated by an Al Kα source (14,867 eV). The diameter of the analyzed region is 10 mm.

TGA characterizations were performed on a TGA 4000 from Perkin Elmer. The ramping rate of temperature was 10 °C·min^{-1}.

Brunauer-Emmett-Teller (BET) surface area and Barrett-Joyner-Halenda (BJH) pore volume (desorption branch) were calculated from N_2-physisorption measurements on a Micromeritics 3Flex apparatus at liquid nitrogen temperature between 10^{-5} and 0.99 relative N_2 pressure. Samples (ca. 150 mg) were dried at 120°C (temperature reached with a ramp of 2°C/min) under vacuum (< 10^{-3} mbar) for 4 h and a leak test was performed prior to analysis.

Working electrode preparation.

To prepare catalyst ink, 3 mg of the sample and 40 μL of Nafion® perfluorinated resin solution (5 wt.%, Sigma) were dispersed in 1 mL of ethanol by ultrasonic treatment for 30 min. Belt-shape carbon cloths (Fuel Cell Store) after the treatment of ultrapure nitric acid were used as the working electrode. The area exposed to the electrolyte was fixed at 1 cm^2 by shading the carbon cloth by sealing film. For SnO/C, SnO_2/C and Sn/C, 100 μL of catalyst ink was loaded on the carbon cloth by drop-drying in 4 times. Thus, the loading of catalyst on carbon cloth was 0.3 $mg \cdot cm^{-2}$. For l-SnO, 500 μL of catalyst ink was loaded on the carbon cloth by drop-drying in 20 times. Thus, the loading of catalyst on carbon cloth was 1.5 $mg \cdot cm^{-2}$.

Electrochemical measurement.

Electrochemical characterizations including CV, LSV and chronoamperometry were carried out on a Gamry Reference 3000 electrochemical instrument using a homemade air-tight two-chamber cell. Working and reference electrodes were fixed in one chamber and counter electrode in the other one. The two chambers were separated by an anion exchange membrane (fumasep® FAA-3-PK-130). Double-junction protected Ag/AgCl electrode with saturated KCl filling solution and Pt wire were used as reference and counter electrodes, respectively. All potentials mentioned in this paper were converted to the value versus RHE by the equation: $E_{vs.RHE} = E_{vs.Ag/AgCl} + 0.197\ V + 0.0592\ V \times pH$. The pH value of the electrolytes was tested by a pH meter (HI 991002, Hanna instruments). 0.5 M $KHCO_3$ electrolyte was prepared by bubbling CO_2 into aqueous solution of 0.25 M K_2CO_3 for 6 hours followed by bubbling N_2 for another 6 hours. The electrolyte in the chamber of working electrode was stirred vigorously during the experiments. Pre-electrolysis under N_2 atmosphere at -1.0 V vs RHE for 2 hours by using a bare carbon cloth as working electrode was conducted before electrochemical measurements. The working electrode side was bubbled with CO_2 or N_2 for at least 30 min to get the electrolyte saturated. The inlet gas was pre-humidified by 0.5 M $KHCO_3$ solution to minimize the evaporation of the electrolyte. 50 cycles of CV sweeps were conducted before the collection of LSV curves. Before the electrolysis tests and double layer capacitance measurements, the catalyst was pre-reduced at -0.66 V for 30 min to reduce SnO or SnO_2 nanoparticles.

Product analysis of CO_2 electroreduction.

The amounts of CO and H_2 generated on the working electrode were quantified by a homemade gas chromatography (GC) equipped with a Carboxen®-1010 PLOT capillary column and a thermal conductivity detector (VICI). The total volume of the chamber of working electrode was 20 mL and 12 mL of electrolyte was added into this chamber. Calibrations of the correlation between the GC peak area and the concentration of CO and H_2 was done first. The electrolyte was bubbled with CO_2 for 30 min and then both the inlet and outlet gas line were closed. A certain volume of CO or H_2 gas was injected into the chamber and the electrolyte was stirred for 30 min to equilibrate the system. Then 1 mL of gas in the headspace was extracted by a syringe and injected into the GC. The analysis of CO and H_2 obtained from electrolysis was done with a similar method: the electrolyte was first bubbled with CO_2 for 30 min before sealing the chamber. Next, the electrolysis was conducted until the integral charge reached -4 Coulomb (if the total current density was lower than 0.5 $mA \cdot cm^{-2}$, electrolysis was stopped as the integral charge reached -1 Coulomb). Then the gas in the headspace was analyzed. Figure S1a shows a typical GC curve. Helium (He) was used as the carrier gas and the column was heated with a temperature program shown in Figure S1b. Figure S1c and S1d show the calibration curves of CO and H_2. Two small peaks correspond to the trace amount of air (O_2 + N_2, total volume fraction < 2%) were observed. The sum of the Faraday efficiencies of H_2, CO and formate was higher than 85% for every single test.

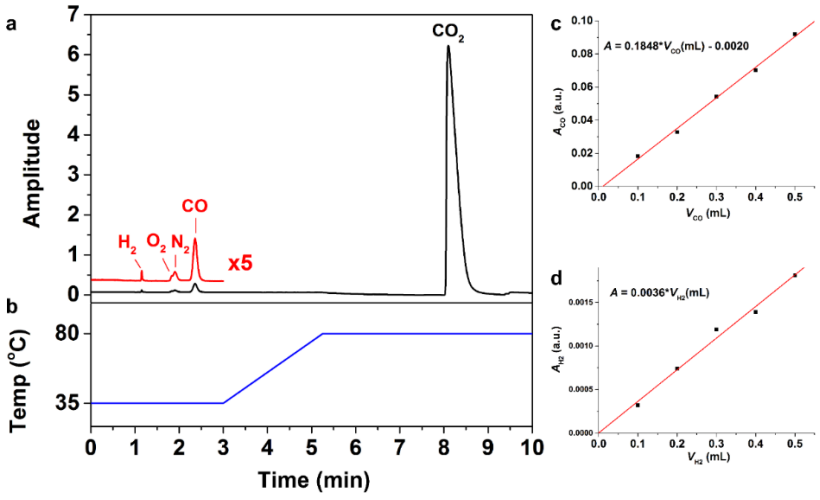

Figure S1. GC analysis of CO and H_2. (a) A typical GC curve of gas extracted from head space of the cell after CO_2 electroreduction experiment. Red curve shows the magnification of the GC curve in first 3 min. (b) The temperature program for the GC analysis. The calibration curve of CO (c) and H_2 (d).

^{1}H-NMR (Bruker, 400 MHz) was used to quantify the amount of formate. The analyses were conducted before and after electrolysis. The integral charge of the electrolysis reached -10 Coulomb for each experiment (if the total current density was lower than 0.5 mA·cm^{-2}, electrolysis was stopped as the integral charge reached -2 Coulomb). 240 μL of the electrolyte was extracted and mixed with 200 μL of dimethyl sulfoxide (DMSO) solution containing 25 ppm (volume fraction) DMSO and 50 μL of D_2O as the sample for 1H-NMR analysis. Figure S2 shows typical ^{1}H-NMR spectra of electrolyte before and after electrolysis.

By testing gas sample with known partial pressure of H_2 and CO, we found the relative error for CO detection by our GC instrument was about 5%. The relative error for H_2 detection was about 10% because of low sensitivity, as shown in Figure S1d. By testing solution samples containing known amount of formate and our internal standard (DMSO), the relative error for formate detection was about 6%. The Faraday efficiency of H_2 on SnO_2/C and Sn/C was comparatively higher, which led to higher error in the Faraday efficiency. However, the Faraday efficiencies of CO and formate, which are the focus of our study, have less errors.

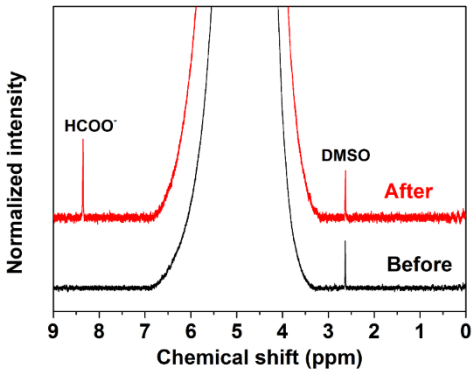

Figure S2. Typical ^{1}H-NMR spectra of electrolyte before (black) and after (red) electrolysis.

CO_2 electroreduction performance

Table S1-1 to S1-8 summarize all the measurement results of CO_2 electroreduction on SnO/C, SnO_2/C, Sn/C and l-SnO/C. Every measurement was repeated 3 times on 3 pieces of working electrodes.

Table S1-1 CO_2 electroreduction performance of SnO/C in CO_2 saturated 0.5 M $KHCO_3$ electrolyte

Potential (V vs RHE)	Total *j* (mA·cm^{-2})	FE of CO (%)	FE of formate (%)	FE of CO + formate (%)	FE of H_2 (%)	*j* of CO (mA·cm^{-2})	*j* of formate (mA·cm^{-2})	j of H_2 (mA·cm^{-2})
-0.46	1.053	17	11	28	60	0.179	0.116	0.632
	1.276	19	8	27	60	0.242	0.102	0.766
	1.181	24	11	35	55	0.283	0.130	0.650
-0.56	4.214	30	18	48	40	1.264	0.758	1.686
	4.989	32	21	53	40	1.596	1.048	1.996
	4.516	39	25	64	25	1.761	1.129	1.129
-0.66	11.115	41	35	76	25	4.557	3.890	2.779
	13.809	39	39	78	20	5.386	5.386	2.762
	12.943	32	39	71	20	4.142	5.048	2.589
-0.76	15.825	32	59	91	8	5.064	9.337	1.266
	17.333	39	49	88	15	6.760	8.493	2.600
	16.448	33	54	87	10	5.428	8.882	1.645
-0.86	27.233	24	75	99	5	6.536	20.425	1.362
	32.511	34	62	96	2	11.054	20.157	0.650
	29.666	27	66	93	5	8.010	19.580	1.483

Table S1-2 CO_2 electroreduction performance of SnO_2/C in CO_2 saturated 0.5 M $KHCO_3$ electrolyte.

Potential (V vs RHE)	Total *j* ($mA \cdot cm^{-2}$)	FE of CO (%)	FE of formate (%)	FE of CO + formate (%)	FE of H_2 (%)	*j* of CO ($mA \cdot cm^{-2}$)	*j* of formate ($mA \cdot cm^{-2}$)	*j* of H_2 ($mA \cdot cm^{-2}$)
-0.46	0.355	6	3	9	80	0.021	0.011	0.284
	0.291	8	3	11	90	0.023	0.009	0.262
	0.319	5	5	10	75	0.016	0.016	0.239
-0.56	1.042	8	8	16	75	0.083	0.083	0.782
	0.808	11	7	18	90	0.089	0.057	0.727
	0.934	7	10	17	75	0.065	0.093	0.700
-0.66	3.732	6	15	21	65	0.224	0.560	2.426
	3.024	5	14	19	85	0.151	0.423	2.570
	3.241	10	11	21	70	0.324	0.357	2.269
-0.76	15.208	6	26	32	55	0.912	3.954	8.364
	13.875	5	21	26	80	0.694	2.914	11.100
	14.116	3	27	30	60	0.423	3.811	8.470
-0.86	34.614	2	61	63	40	0.692	21.115	13.846
	27.879	5	52	57	25	1.394	14.497	6.970
	29.770	4	50	54	25	1.191	14.885	7.442

Table S1-3 CO_2 electroreduction performance of Sn/C in CO_2 saturated 0.5 M $KHCO_3$ electrolyte

Potential (V vs RHE)	Total *j* ($mA \cdot cm^{-2}$)	FE of CO (%)	FE of formate (%)	FE of CO + formate (%)	FE of H_2 (%)	*j* of CO ($mA \cdot cm^{-2}$)	*j* of formate ($mA \cdot cm^{-2}$)	*j* of H_2 ($mA \cdot cm^{-2}$)
-0.46	0.181	5	10	15	70	0.009	0.018	0.127
	0.158	6	13	19	80	0.009	0.021	0.126
	0.154	3	12	15	70	0.005	0.018	0.108
-0.56	0.902	7	12	19	60	0.063	0.108	0.541
	0.784	4	10	14	80	0.031	0.078	0.627
	0.715	5	12	17	70	0.036	0.086	0.500
-0.66	2.273	8	46	54	30	0.182	1.046	0.682
	1.893	13	40	53	45	0.246	0.757	0.852
	1.722	13	37	50	45	0.224	0.637	0.775
-0.76	2.524	25	50	75	20	0.631	1.262	0.505
	2.256	24	55	79	10	0.541	1.241	0.226
	2.119	18	61	79	10	0.381	1.293	0.212
-0.86	4.103	11	77	88	20	0.451	3.159	0.821
	3.754	20	70	90	10	0.751	2.628	0.375
	3.356	17	67	84	20	0.571	2.249	0.671

Table S1-4 CO_2 electroreduction performance of I-SnO/C in CO_2 saturated 0.5 M $KHCO_3$ electrolyte.

Potential (V vs RHE)	Total *j* ($mA \cdot cm^{-2}$)	FE of CO (%)	FE of formate (%)	FE of CO + formate (%)	FE of H_2 (%)	*j* of CO ($mA \cdot cm^{-2}$)	*j* of formate ($mA \cdot cm^{-2}$)	*j* of H_2 ($mA \cdot cm^{-2}$)
-0.46	1.043	6	19	25	70	0.063	0.198	0.730
	1.336	9	24	33	55	0.120	0.321	0.735
	1.287	9	23	32	60	0.116	0.296	0.772
-0.56	5.088	15	32	47	40	0.763	1.628	2.035
	5.814	10	39	49	40	0.581	2.267	2.326
	5.639	14	41	55	30	0.789	2.312	1.692
-0.66	13.244	16	49	65	25	2.119	6.490	2.649
	16.570	12	56	68	20	1.988	9.279	4.971
	15.433	17	46	63	30	2.624	7.099	3.858
-0.76	18.542	22	67	89	10	4.079	12.423	1.854
	23.221	14	73	87	5	3.251	16.951	1.161
	20.434	17	77	94	5	3.474	15.734	1.022
-0.86	31.009	18	74	92	5	5.582	22.947	1.550
	38.225	14	80	94	2	5.352	30.580	0.764
	33.026	16	72	88	10	5.284	23.779	3.303

Table S1-5 CO_2 electroreduction performance of SnO/C at -0.66 V vs RHE in CO_2 saturated 0.5 M K_2HPO_4, 0.5 M $KHCO_3$ and 0.5 M KCl.

Electrolyte	Total *j* ($mA \cdot cm^{-2}$)	FE of CO (%)	FE of formate (%)	FE of CO + formate (%)	FE of H_2 (%)	*j* of CO ($mA \cdot cm^{-2}$)	*j* of formate ($mA \cdot cm^{-2}$)	*j* of H_2 ($mA \cdot cm^{-2}$)
K_2HPO_4	16.384	24	47	71	25	3.931	7.699	4.095
	18.957	29	39	68	28	5.498	7.394	5.309
	20.053	25	39	64	32	5.012	7.820	6.416
$KHCO_3$	11.115	41	35	76	25	4.557	3.890	2.779
	13.809	39	39	78	20	5.386	5.386	2.762
	12.943	32	39	71	20	4.142	5.048	2.589
KCl	1.042	76	19	95	4	0.790	0.198	0.042
	1.214	70	24	94	3	0.847	0.290	0.036
	1.308	73	25	98	1	0.956	0.328	0.013

Table S1-6 Data for Tafel plots of SnO/C in CO_2 saturated 0.5 M $KHCO_3$ electrolyte.

Potential (V vs RHE)	Total *j* ($mA \cdot cm^{-2}$)	FE of CO (%)	FE of formate (%)	FE of CO + formate (%)	FE of H_2 (%)	*j* of CO ($mA \cdot cm^{-2}$)	*j* of formate ($mA \cdot cm^{-2}$)	*j* of H_2 ($mA \cdot cm^{-2}$)
-0.46	0.138	15	1	16	70	0.021	0.001	0.097
	0.121	15	2	17	90	0.018	0.002	0.109
	0.113	14	1	15	70	0.016	0.001	0.079
-0.56	0.438	14	4	18	70	0.061	0.018	0.307
	0.505	19	4	23	60	0.096	0.020	0.303
	0.417	16	3	19	80	0.067	0.013	0.334
-0.66	1.053	17	11	28	60	0.179	0.116	0.632
	1.276	19	8	27	60	0.242	0.102	0.766
	1.181	24	11	35	55	0.283	0.130	0.650
-0.76	2.392	24	16	40	50	0.574	0.383	1.196
	3.011	33	15	48	40	0.994	0.452	1.204
	2.434	29	10	39	55	0.706	0.243	1.339

Table S1-7 CO_2 electroreduction performance of l-SnO/C at -0.66 V vs RHE in CO_2 saturated $KHCO_3$-KCl electrolyte.

Electrolyte	Total *j* ($mA \cdot cm^{-2}$)	FE of CO (%)	FE of formate (%)	FE of CO + formate (%)	FE of H_2 (%)	*j* of CO ($mA \cdot cm^{-2}$)	*j* of formate ($mA \cdot cm^{-2}$)	*j* of H_2 ($mA \cdot cm^{-2}$)
0.5 M $KHCO_3$	15.433	17	46	63	25	2.624	7.099	3.858
	13.244	16	49	65	20	2.119	6.490	2.649
	16.570	12	56	68	30	1.988	9.279	4.971
0.25 M KCl + 0.25 M $KHCO_3$	8.234	21	59	80	14	1.728	4.858	1.152
	7.880	23	50	73	21	1.812	3.940	1.655
	8.439	27	55	82	12	2.279	4.642	1.013
0.375 M KCl + 0.125 M $KHCO_3$	5.073	33	51	84	13	1.673	2.586	0.659
	4.726	31	58	89	8	1.466	2.743	0.378
	5.374	37	48	85	14	1.987	2.578	0.752
0.438 M KCl + 0.062 M $KHCO_3$	3.209	44	49	93	5	1.412	1.573	0.160
	3.025	48	43	91	6	1.450	1.299	0.181
	3.407	39	47	86	9	1.330	1.603	0.307
0.469 M KCl + 0.031 M $KHCO_3$	2.112	59	36	95	3	1.245	0.760	0.063
	1.954	51	40	91	6	0.994	0.780	0.117
	2.295	54	41	95	3	1.242	0.943	0.069

Table S1-8 CO_2 electroreduction performance of SnO/C at -0.66 V vs RHE in CO_2 saturated $KHCO_3$-KCl electrolyte.

Electrolyte	Total *j* ($mA \cdot cm^{-2}$)	FE of CO (%)	FE of formate (%)	FE of CO + formate (%)	FE of H_2 (%)	*j* of CO ($mA \cdot cm^{-2}$)	*j* of formate ($mA \cdot cm^{-2}$)	*j* of H_2 ($mA \cdot cm^{-2}$)
0.5 M $KHCO_3$	11.115	41	35	76	25	4.557	3.890	2.779
	12.943	32	39	71	20	4.142	5.048	2.589
	13.809	39	39	78	20	5.386	5.386	2.762
0.25 M KCl + 0.25 M $KHCO_3$	7.554	43	39	82	14	3.246	2.944	1.057
	8.008	51	34	85	12	4.085	2.723	0.961
	8.669	46	32	78	17	3.988	2.774	1.474
0.375 M KCl + 0.125 M $KHCO_3$	5.532	59	34	93	10	3.263	1.880	0.553
	5.060	57	27	84	11	2.884	1.366	0.557
	4.815	52	30	82	7	2.506	1.446	0.337
0.438 M KCl + 0.062 M $KHCO_3$	3.363	60	24	84	11	2.016	0.806	0.370
	3.110	65	29	94	4	2.022	0.902	0.124
	2.949	62	28	90	8	1.829	0.826	0.236
0.469 M KCl + 0.031 M $KHCO_3$	2.033	66	27	93	6	1.340	0.548	0.122
	1.945	71	22	93	4	1.377	0.427	0.078
	1.820	67	25	92	6	1.219	0.455	0.109

2. Statistical Method of Averaged Particle-Centered Radial Distribution Diagrams of Particle Density

For one particle A, the particle-centered radial particle density ($d_A(R)$) is defined as the particle density in a ring with the radius of R centered at A, expressed as:

$$d_A(R) = \frac{N(R-\frac{\Delta r}{2} < r_{A-X} < R+\frac{\Delta r}{2})}{A(\text{ring})} = \frac{N(R-\frac{\Delta r}{2} < r_{A-X} < R+\frac{\Delta r}{2})}{2\pi R\Delta r}$$

In this expression, A(ring) is the area of this ring and $r_{A\text{-}X}$ is the distance between particle A and X. $N(R-\frac{\Delta r}{2} < r_{A-X} < R+\frac{\Delta r}{2})$ is the number of particles in the ring with the width of Δr, namely the number of particles with the distance from A between $(R-\frac{\Delta r}{2})$ and $(R+\frac{\Delta r}{2})$.

Regions containing more than 170 particles were used in the analysis. The averaged particle-centered radial particle density ($\bar{d}(R)$) is expressed as:

$$\bar{d}(R) = \frac{\sum_{M\in N} d_M(R)}{N} = \frac{\sum_{M\in N} N(R-\frac{\Delta r}{2} < r_{M-X} < R+\frac{\Delta r}{2})}{2N\pi R\Delta r}$$

In this expression, N is the set of all particles and N is the number of particles. Then, $\sum_{M\in N} N(R-\frac{\Delta r}{2} < r_{M-X} < R+\frac{\Delta r}{2})$ is two times of the number of interparticle distance in the range between $(R-\frac{\Delta r}{2})$ and $(R+\frac{\Delta r}{2})$ since every interparticle distance was counted twice. By measuring all the interparticle distances in the region, the averaged particle-centered radial distribution diagrams of particle density were depicted. Δr was set to 1 nm in these diagrams.

Figure S3 shows the HAADF-STEM images and corresponding averaged particle-centered radial distribution diagrams of particle density of SnO/C (a), l-SnO/C (b) and SnO_2/C (c). Red dots on HAADF-STEM images depict the centers of nanoparticles. Due to the boundary of the selected area, generally, particle density decreased as the radius increased. These diagrams on one hand show how crowded nanoparticles were distributed on carbon black, and on the other hand reflect the homogeneity of the distribution. If nanoparticles were distributed homogeneously, the particle density shows a gradual decrease as the radius increases. On the contrary, if nanoparticles aggregate in some parts, the maximum particle density appears at a short radius followed by a sudden drop as the radius increases. Therefore, it can be concluded that the homogeneity of nanoparticle distribution of SnO/C is higher than that of l-SnO/C, and further higher than that of SnO_2/C.

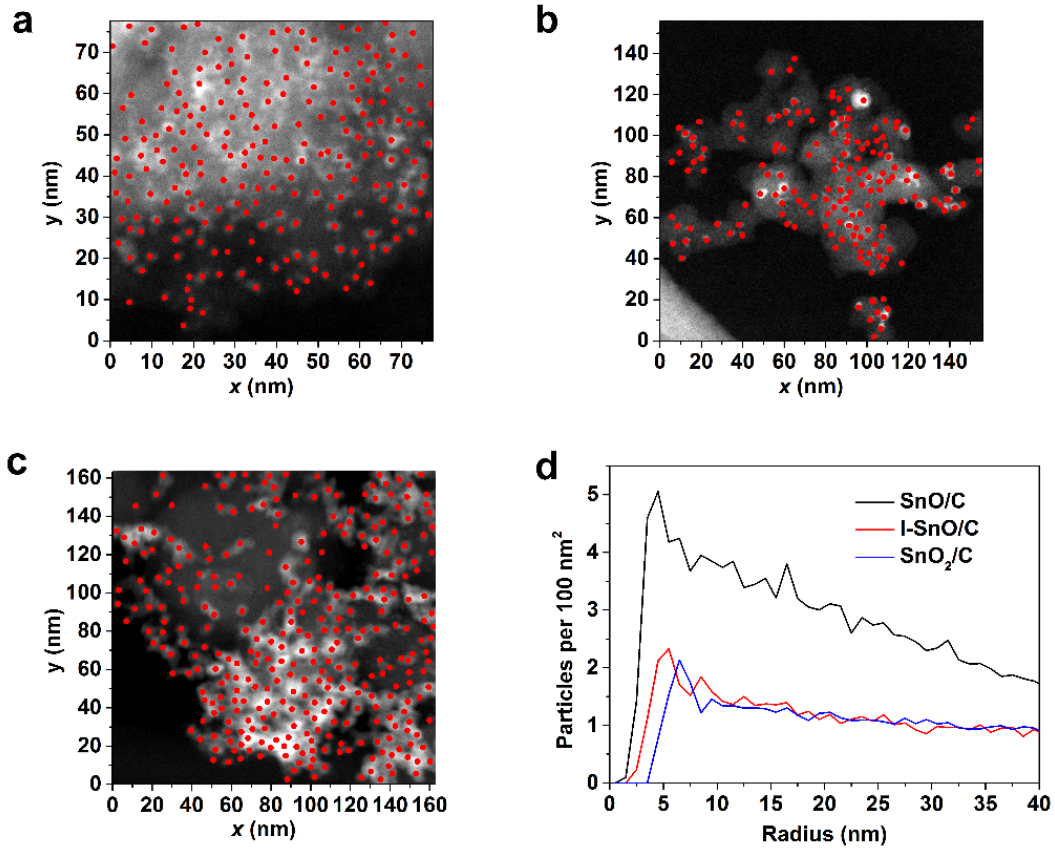

Figure S3. HAADF-STEM images of SnO/C (a), I-SnO/C (b) and SnO_2/C (c). Red dots on HAADF-STEM images depict the centers of nanoparticles. (d) Corresponding averaged particle-centered radial distribution diagrams of particle density.

3. Supplementary Figures and Tables

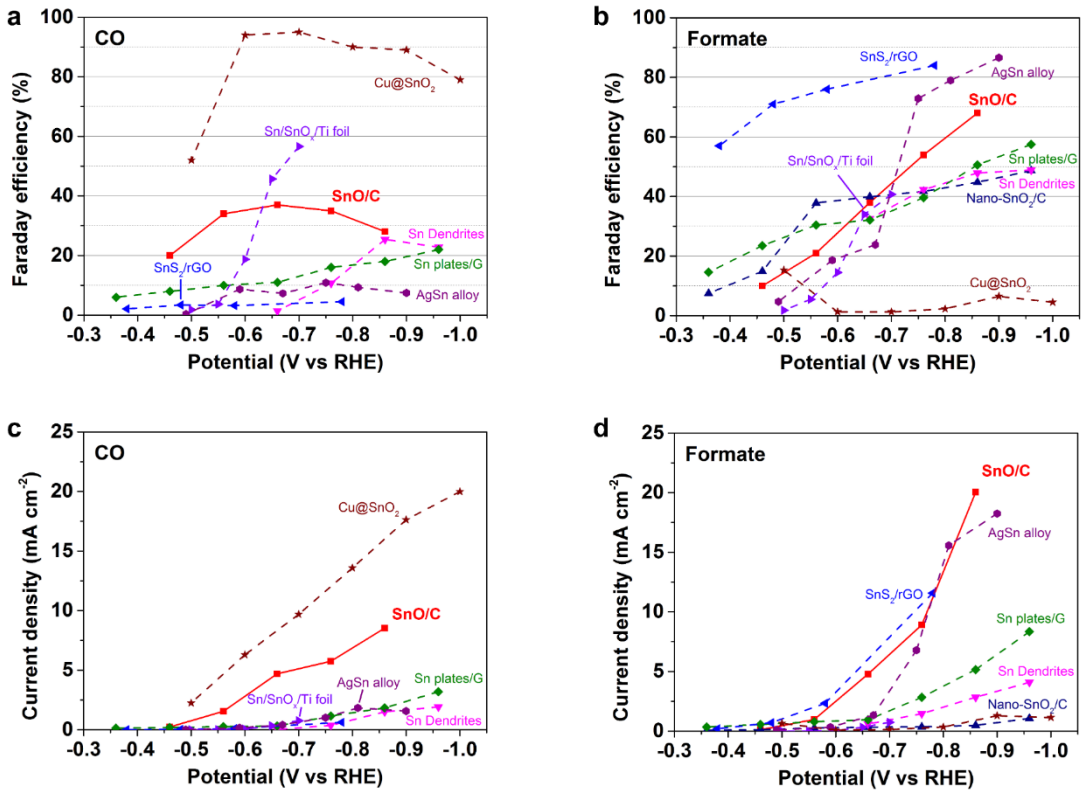

Figure S4. Comparison of the CO_2 electroreduction performance of SnO/C in this paper (red square solid lines, loading of Sn: 120 μg· cm^{-2}) with other Sn-based catalysts in literatures (dashed lines). Faraday efficiency of CO (a) and formate (b). Partial current density of the generation of CO (c) and formate (d). Sn-based catalysts include: carbon black supported nano-sized SnO_2 (Nano-SnO_2/C, dark blue triangles, loading of Sn: 50 μg· cm^{-2}),[1] electrochemically grown dendritic Sn electrode (Sn dendrites, pink triangles),[2] graphene confined Sn nanoplates (Sn plates/G, green diamonds, loading of Sn: 105 μg· cm^{-2}),[3] reduced graphene oxide supported SnS_2 nanoplates (SnS_2/rGO, blue triangles, loading of Sn: 56 μg· cm^{-2}),[4] electro-deposited Sn/SnOx on Ti foil (Sn/SnO_x/Ti foil, violet triangles),[5] $Ag_{76}Sn_{24}$ alloy nanoparticles (AgSn alloy, purple circles, loading of metals: 1 mg·cm^{-2})[6] and Cu-SnO_2 core-shell nanoparticles (Cu@SnO_2, brown stars, loading of metals: 13 mg·cm^{-2}).[7]

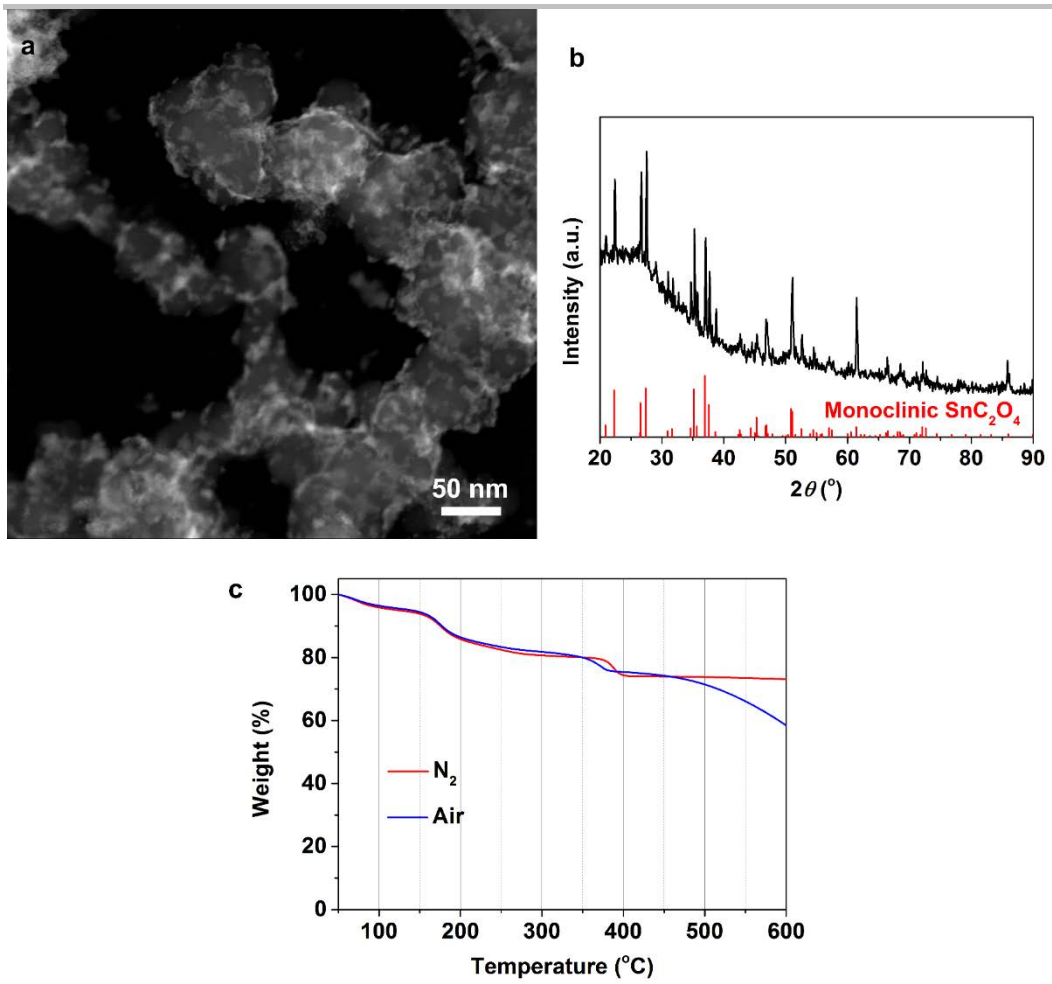

Figure S5. Characterizations of SnC_2O_4/C. (a) HAADF-STEM image. (b) XRD pattern. Red vertical lines indicate the standard diffraction peaks of monoclinic SnC_2O_4 (JCPDS no. 51-0614). (c) TGA curves in N_2 (red) and air (blue) atmosphere. At 400 °C, SnC_2O_4 decomposed completely. Further increase of temperature led to combustion of carbon black in air.

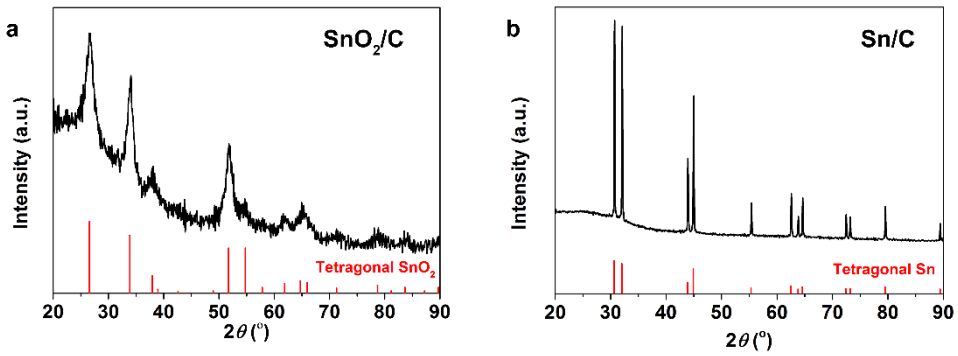

Figure S6. XRD patterns of SnO_2/C (a) and Sn/C (b). Vertical lines in (a) and (b) indicate the standard diffraction patterns of tetragonal SnO_2 (JCPDS no. 05-0467) and tetragonal Sn (JCPDS no. 04-0673), respectively.

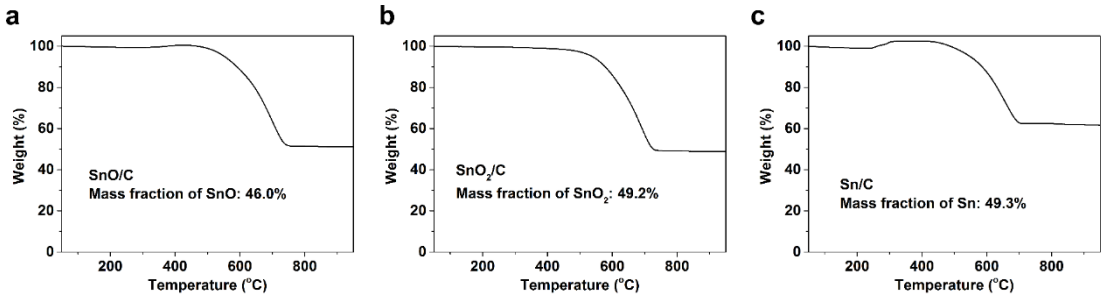

Figure S7. TGA curves of SnO/C (a), SnO_2/C (b) and Sn/C (c) in air atmosphere. The loadings of SnO, SnO_2 and Sn in the composites were determined by these curves, by assuming SnO_2 was the only pyrolysis product at the end of TGA experiments

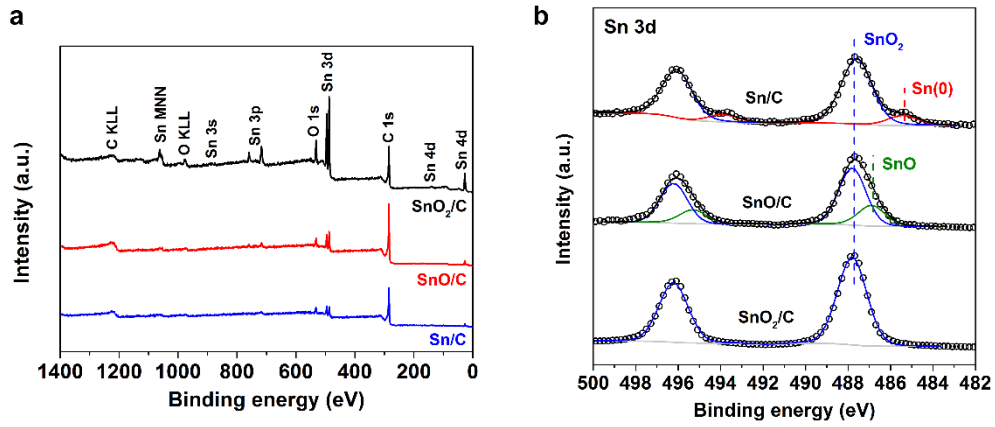

Figure S8 Survey (a) and high-resolution Sn 3d (b) XPS spectra of Sn/C, SnO/C and SnO_2/C. In the high-resolution Sn 3d spectra, black circles show the original data. Grey, blue, green and red curves show the backgrounds, contributions of SnO_2, SnO and metallic Sn species, respectively. Black curves in the spectra of SnO/C and Sn/C show the envelope curves. Doublets located at 487.8 eV and 496.2 eV are ascribed to Sn 3d3/2 and Sn 3d5/2 ionizations in SnO_2 species, which were observed in all the spectra of Sn/C, SnO/C and SnO_2/C.[1] The doublet located at 486.9 eV and 495.3 eV in the spectra of SnO/C is originated from SnO species.[8] The doublet at 485.4 eV and 493.8 eV in the spectra of Sn/C is originated from metallic Sn. This result indicates that the surfaces of Sn and SnO in Sn/C and SnO/C were partially oxidized to form SnO_2 species as they were exposed to air. The fitting results were shown in Table S2.

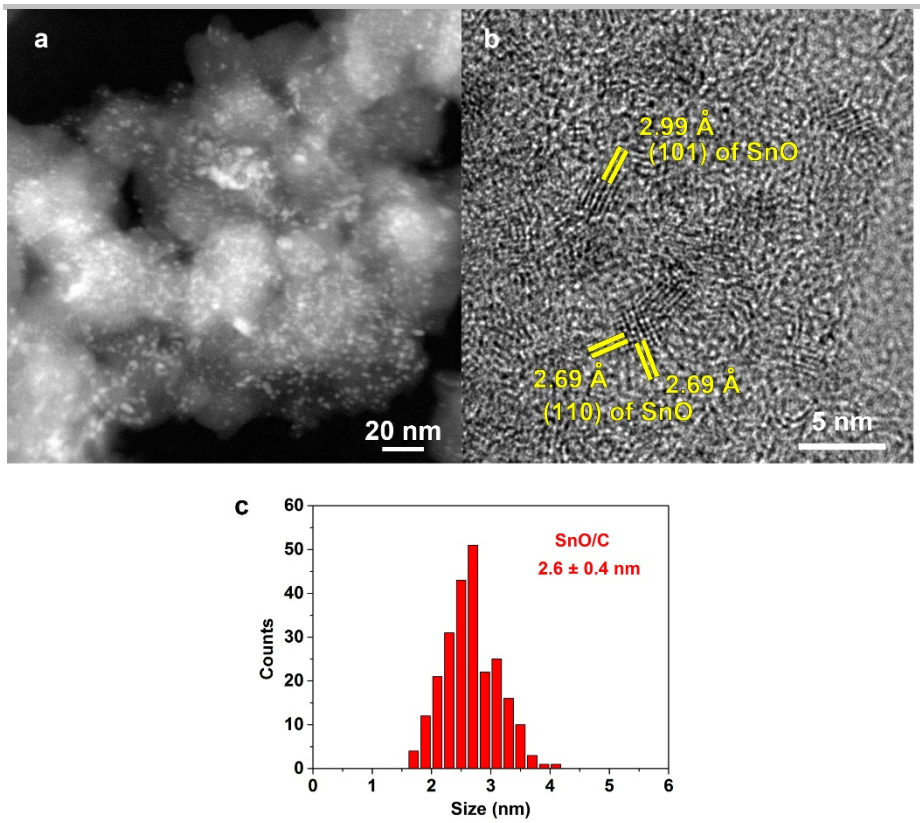

Figure S9. (a) Large-area HAADF-STEM image of SnO/C. (b) HRTEM image of SnO/C. Lattice fringes of tetragonal SnO are highlighted by yellow lines. (c) Particle size distribution diagram of SnO/C.

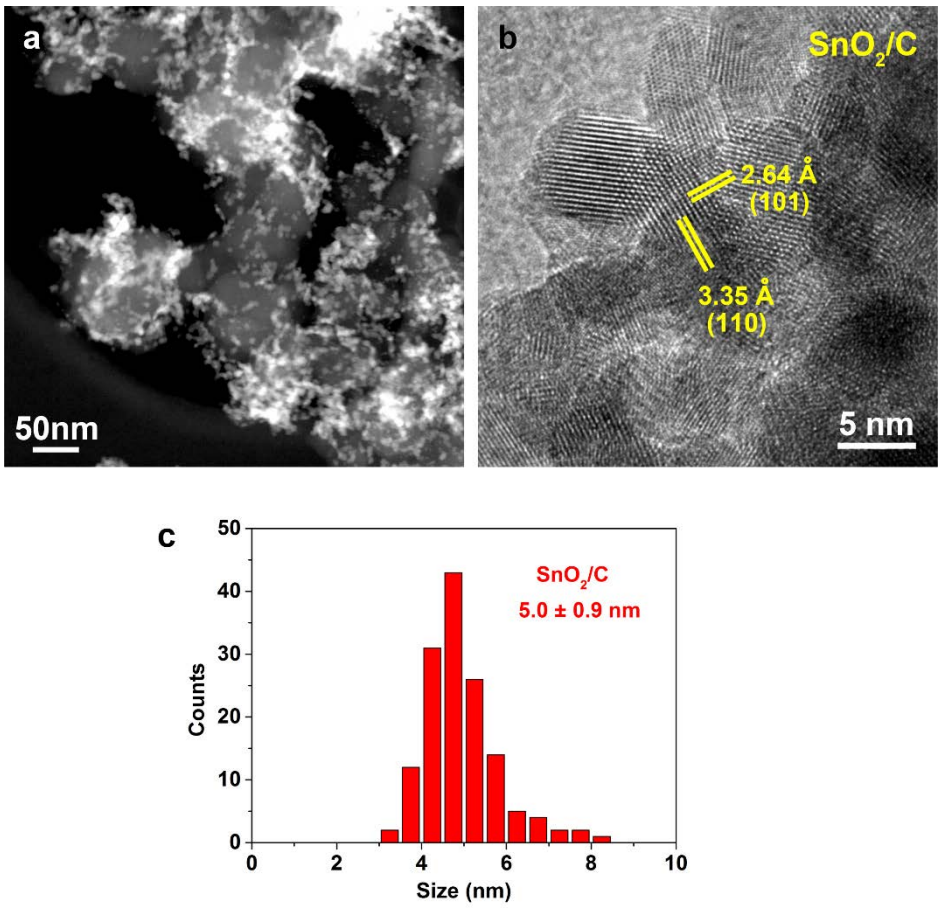

Figure S10. HAADF-STEM (a) and HRTEM (b) images of SnO_2/C. Lattice fringes of tetragonal SnO_2 are highlighted by yellow lines. (c) Particle size distribution diagram of SnO_2/C.

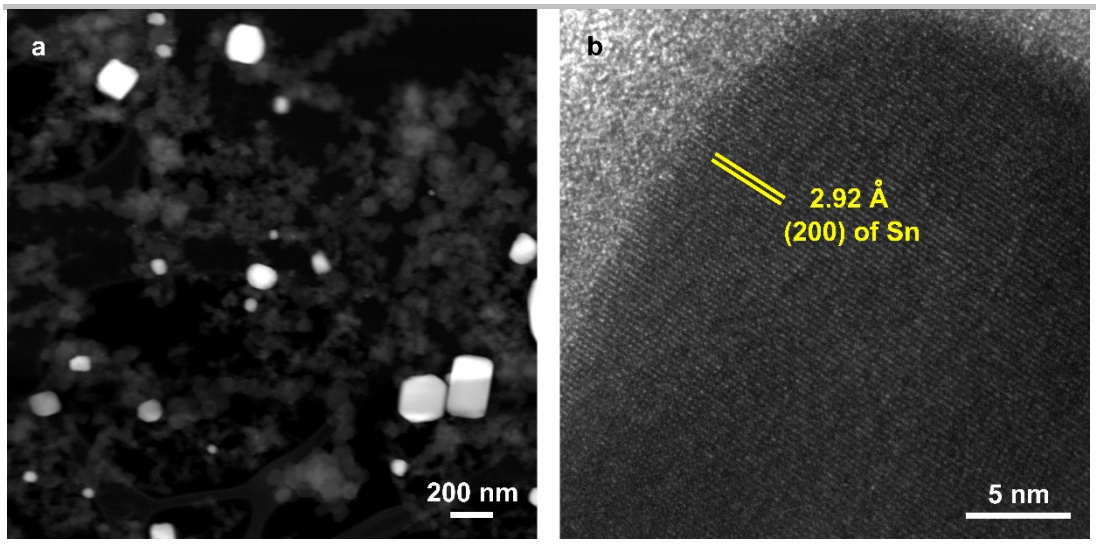

Figure S11. HAADF-STEM (a) and HRTEM (b) images of Sn/C. Lattice fringes of tetragonal Sn are highlighted by yellow lines.

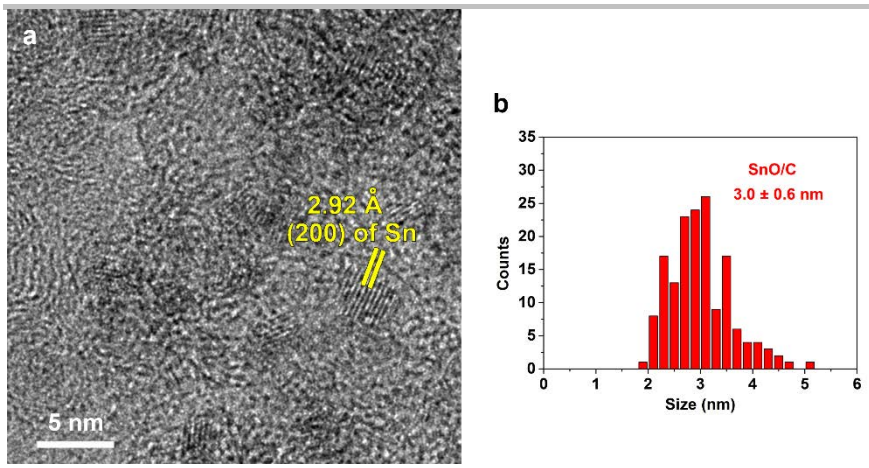

Figure S12. HRTEM image (a) and particle size distribution diagram (b) of SnO/C after electrolysis at -0.66 V vs RHE in CO_2 saturated 0.5 M $KHCO_3$ electrolyte for 1800 s. In panel (a), lattice fringes of tetragonal Sn are highlighted by yellow lines.

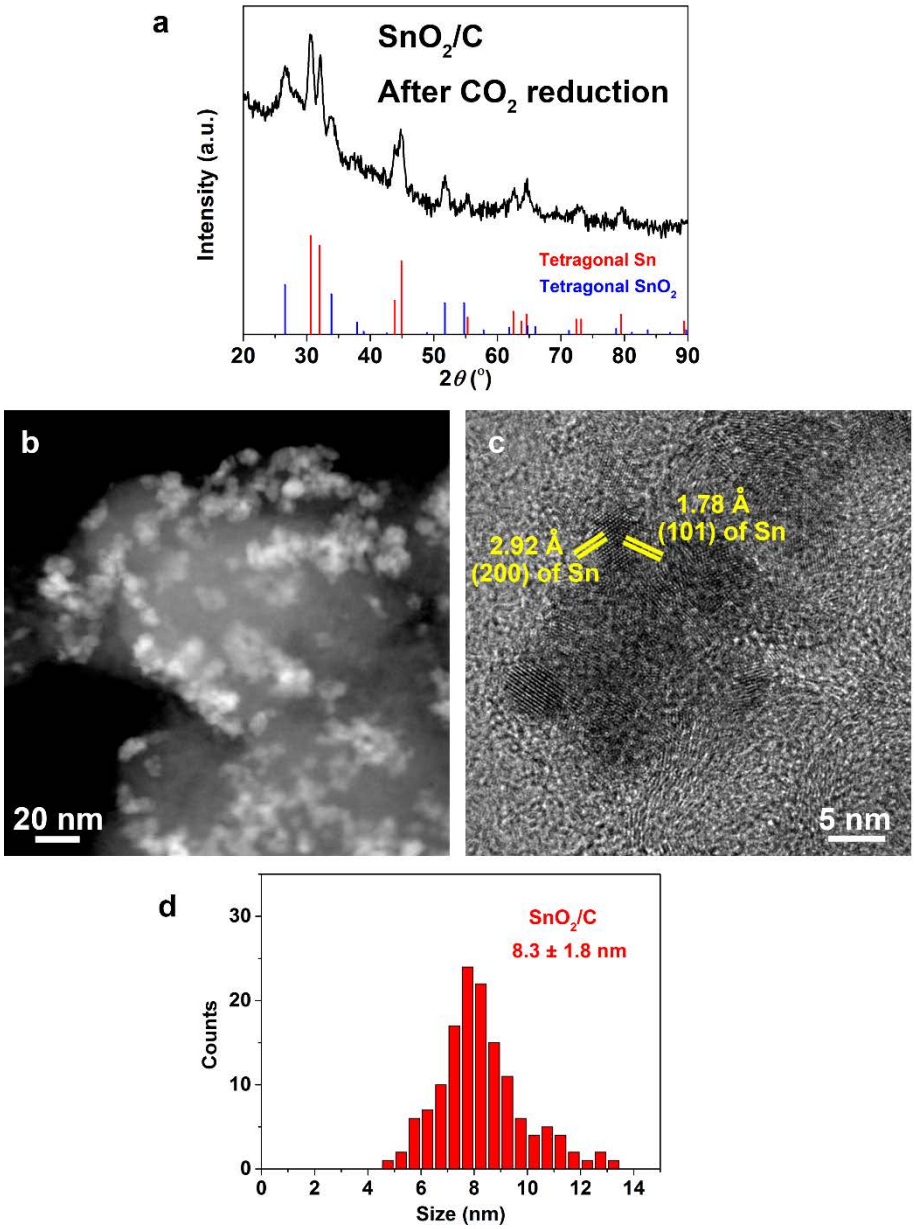

Figure S13. XRD pattern (a) HAADF-STEM (b), HRTEM (c) images and particle size distribution diagram (d) of SnO_2/C after electrolysis at -0.66 V vs RHE in CO_2 saturated 0.5 M $KHCO_3$ electrolyte for 1800 s. In panel (a), Red and blue vertical lines indicate the standard diffraction patterns of tetragonal Sn (JCPDS no. 04-0673) and tetragonal SnO_2 (JCPDS no. 05-0467), respectively. In panel (c), lattice fringes of tetragonal Sn are highlighted by yellow lines.

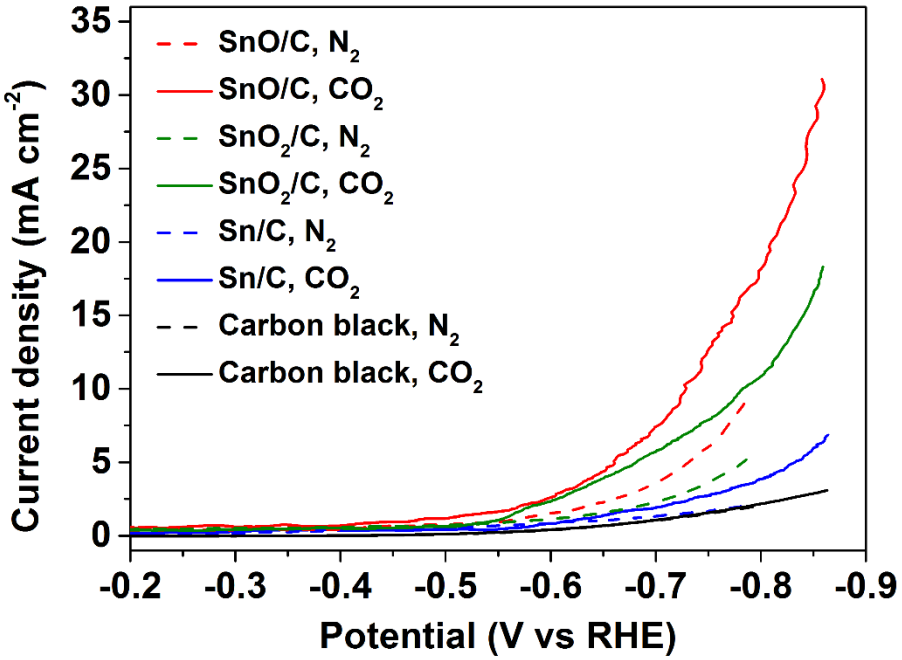

Figure S14. Stable LSV curves of SnO/C (red), SnO_2/C (green), Sn/C (blue) and carbon black (black) in CO_2 saturated (solid curves) and N_2 saturated (dashed curves) 0.5 M $KHCO_3$ electrolyte. The loadings of SnO/C, SnO_2/C and Sn/C were 0.3 mg·cm^{-2} and that of carbon black was 0.15 mg·cm^{-2}. Cathodic sweeps with scan rate of 20 mV· s^{-1} were conducted.

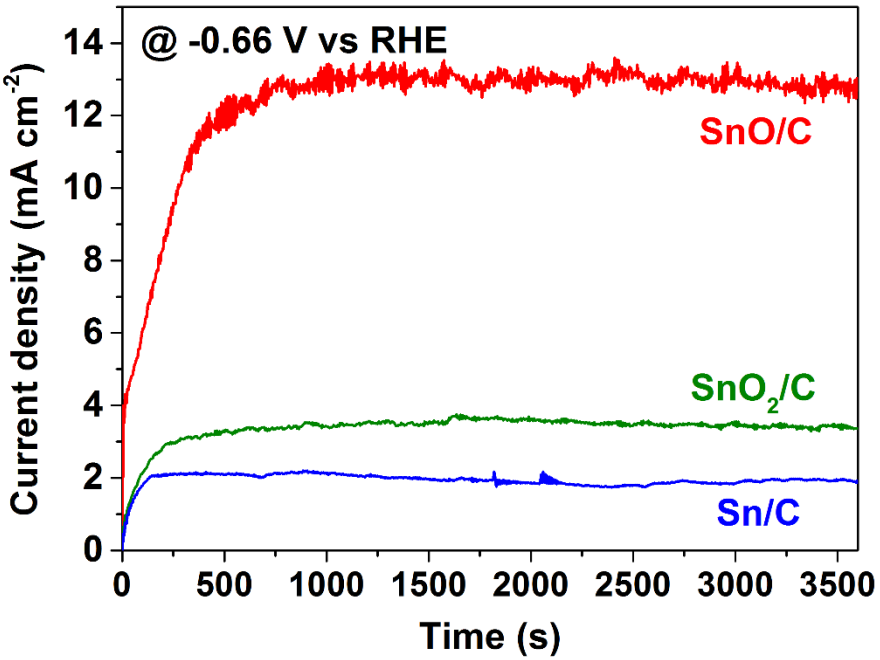

Figure S15. Chronoamperometry curves of SnO/C (red), SnO_2/C (green) and Sn/C (blue) at -0.66 V vs RHE in CO_2 saturated 0.5 M $KHCO_3$ electrolyte.

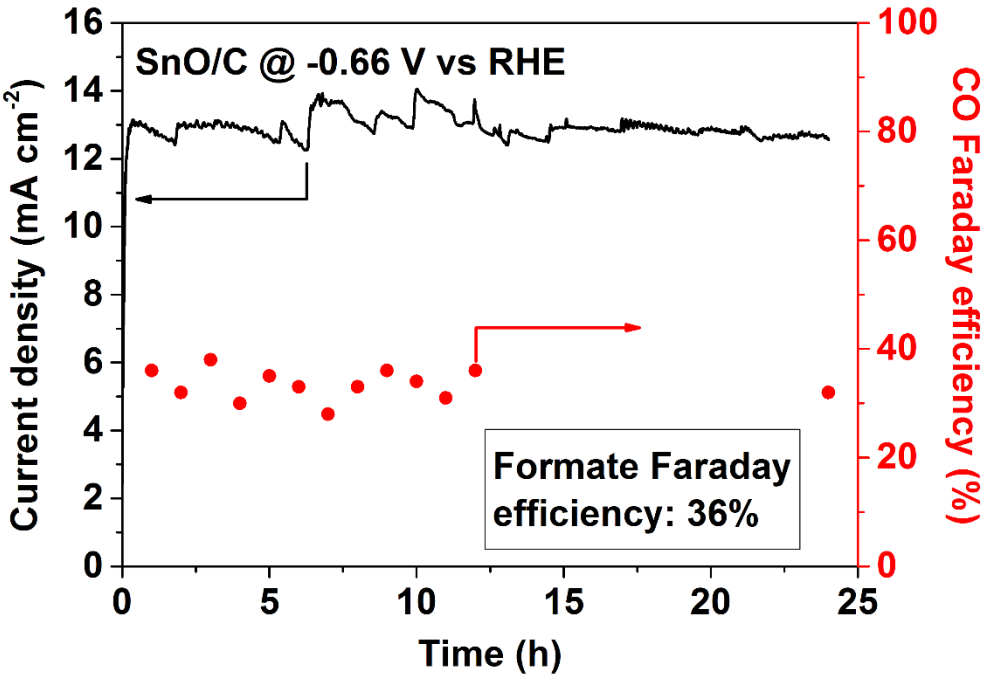

Figure S16. 1-day chronoamperometry curve of SnO/C. Red dots show Faraday efficiency of CO formation. The small fluctuation of the current density was caused by the escape of large bubbles from the working electrode and the disturbance from extracting gas from the head space of the cell by syringe for GC analysis.

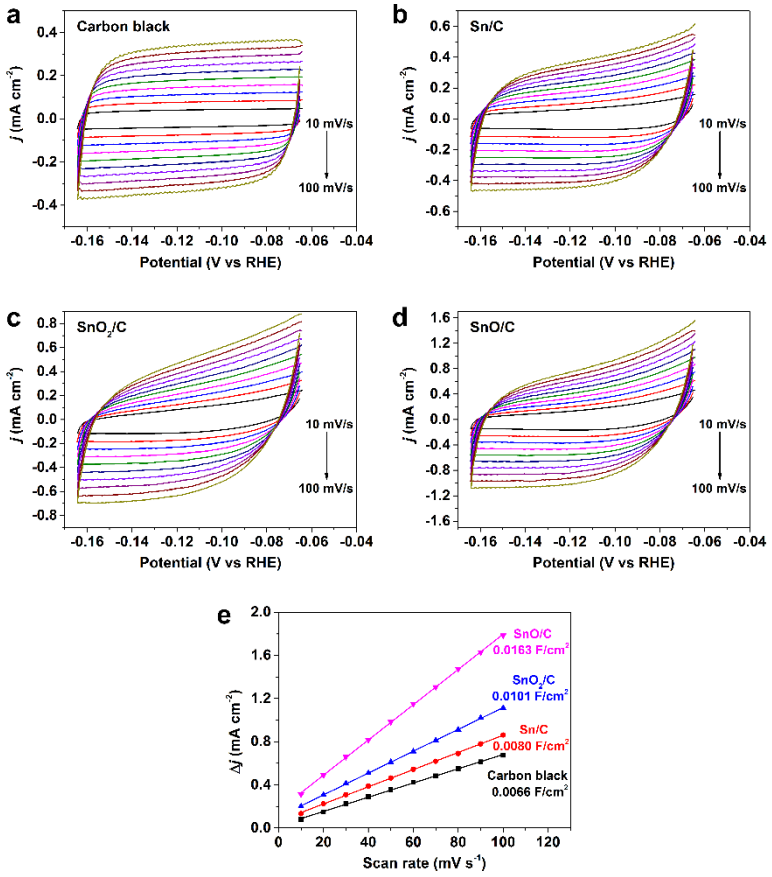

Figure S17. Double layer capacitance obtained from CV measurements. CV curves of carbon black (a), Sn/C (b), SnO_2/C (c) and SnO/C (d) in CO_2 saturated 0.5 M $KHCO_3$ electrolyte between -0.065 V and -0.165 V vs RHE. The loading of carbon black was 0.15 mg·cm^{-2} and those of Sn/C, SnO_2/C and SnO/C were 0.3 mg·cm^{-2}. (e) Current density difference between cathodic and anodic sweeps at -0.115 V vs RHE against scan rate. The double layer capacitances were the slopes of linear fit.

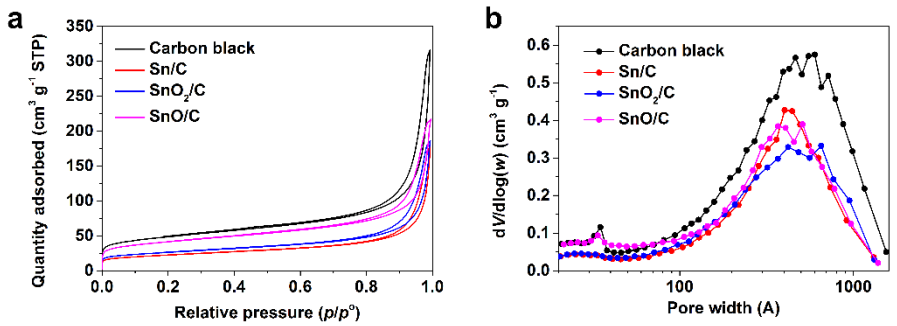

Figure S18. N_2 physisorption experiments of carbon black (black), Sn/C (red), SnO2/C (blue) and SnO/C (pink). (a) N_2 physisorption isothermals. (b) BJH pore size distributions. BET surface areas were calculated based on N_2 physisorption isothermals and listed in Table S3.

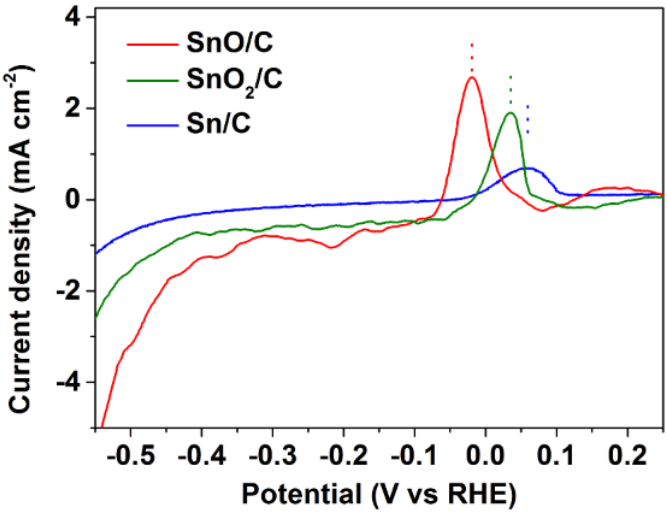

Figure S19. Oxidative LSV curves of SnO/C (red), SnO_2/C (green) and Sn/C (blue) in N_2 saturated 0.1 M KOH electrolyte. The scan rate was 50 $mV \cdot s^{-1}$. The samples were pre-reduced at -0.66 V vs RHE in CO_2 saturated 0.5 M $KHCO_3$ electrolyte for 1800 s before the tests. A peak corresponding to the oxidative adsorption of OH^- was observed in each curve. The dashed vertical lines indicate the maximums of the oxidative peaks. The potential of the peak maximum on SnO/C was 54 mV and 81 mV more negative than that of SnO_2/C and Sn/C, respectively.

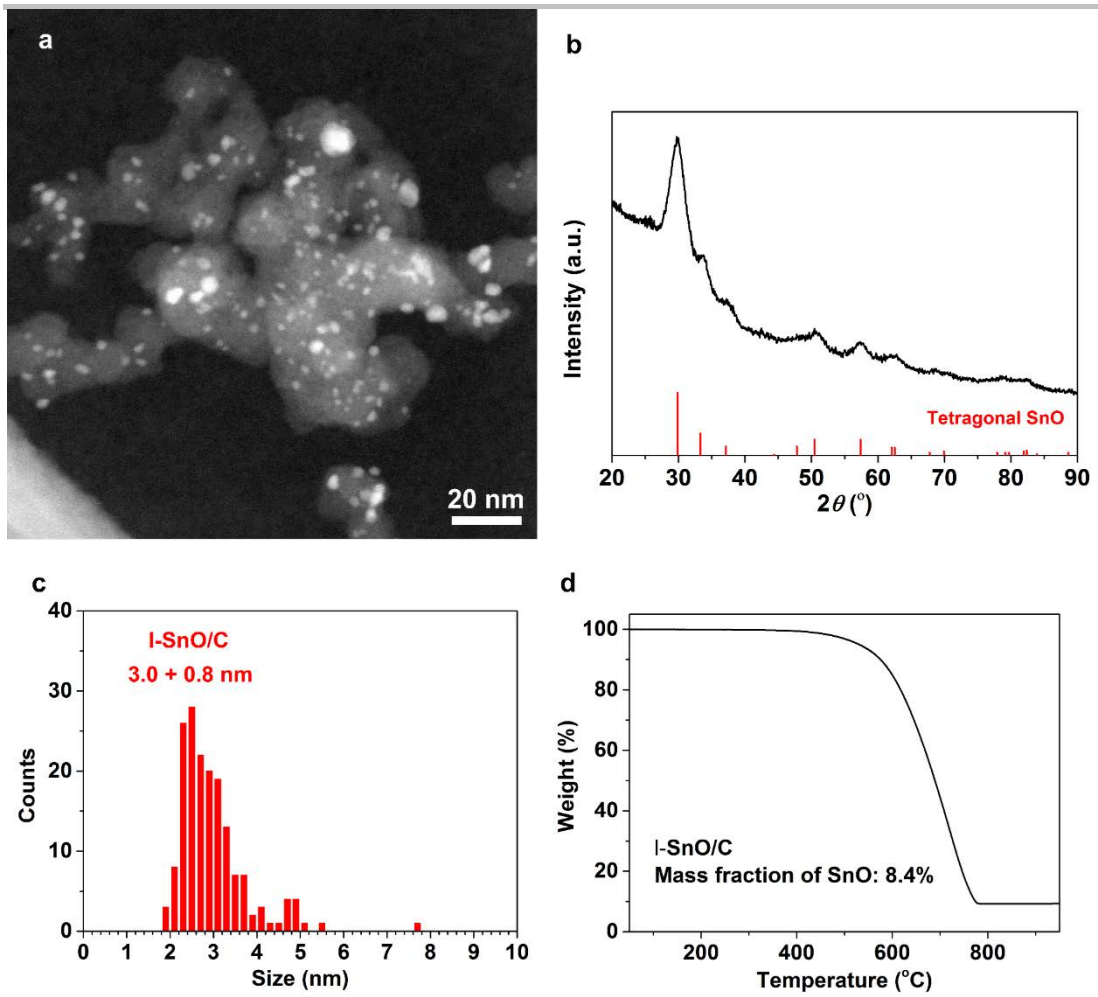

Figure S20. Characterizations of l-SnO/C. (a) HAADF-STEM image. (b) XRD pattern. Red vertical lines indicate the standard diffraction peaks of tetragonal SnO (JCPDS no. 06-0395). (c) Particle size distribution diagram. (d) TGA curve in air atmosphere.

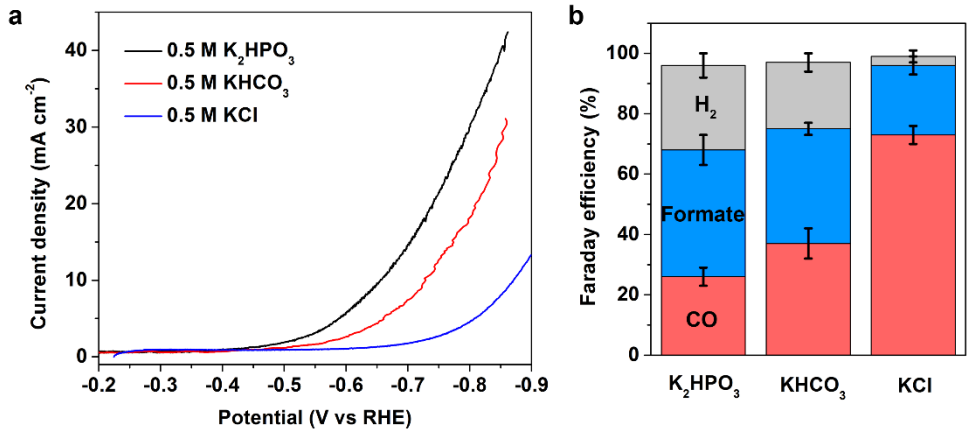

Figure S21. (a) Stable LSV curves of SnO/C in CO_2 saturated 0.5 M K_2HPO_4 (black), 0.5 M $KHCO_3$ (red) and 0.5 M KCl (blue). Cathodic sweeps with scan rate of 20 mV· s^{-1} were conducted. (b) Faraday efficiency of CO (red), formate (blue) and H_2 (grey) in three kinds of electrolytes at -0.66 V vs RHE. KCl has no buffer capacity; $KHCO_3$ shows the buffer capacity through the reaction: $HCO_3^- + OH^- \rightarrow CO_3^{2-} + H_2O$; 0.5 M K_2HPO_4 has stronger buffer capacity than 0.5 M $KHCO_3$, because after the saturation of CO_2, 0.5 M K_2HPO_4 electrolyte transforms to 0.5 M KH_2PO_4 + 0.5 M $KHCO_3$ through the reaction: $HPO_4^{2-} + CO_2 + H_2O \rightarrow H_2PO_4^- + HCO_3^-$. KH_2PO_4 provides additional buffer capacity through the reaction: $H_2PO_4^- + OH^- \rightarrow HPO_4^{2-} + H_2O$. Therefore, 0.5 M K_2HPO_4 electrolyte shows the highest buffer capacity and 0.5 M KCl electrolyte shows the lowest buffer capacity. As the buffer capacity of the electrolyte decreased, the current density at a certain potential decreased, and the Faraday efficiency of CO increased.

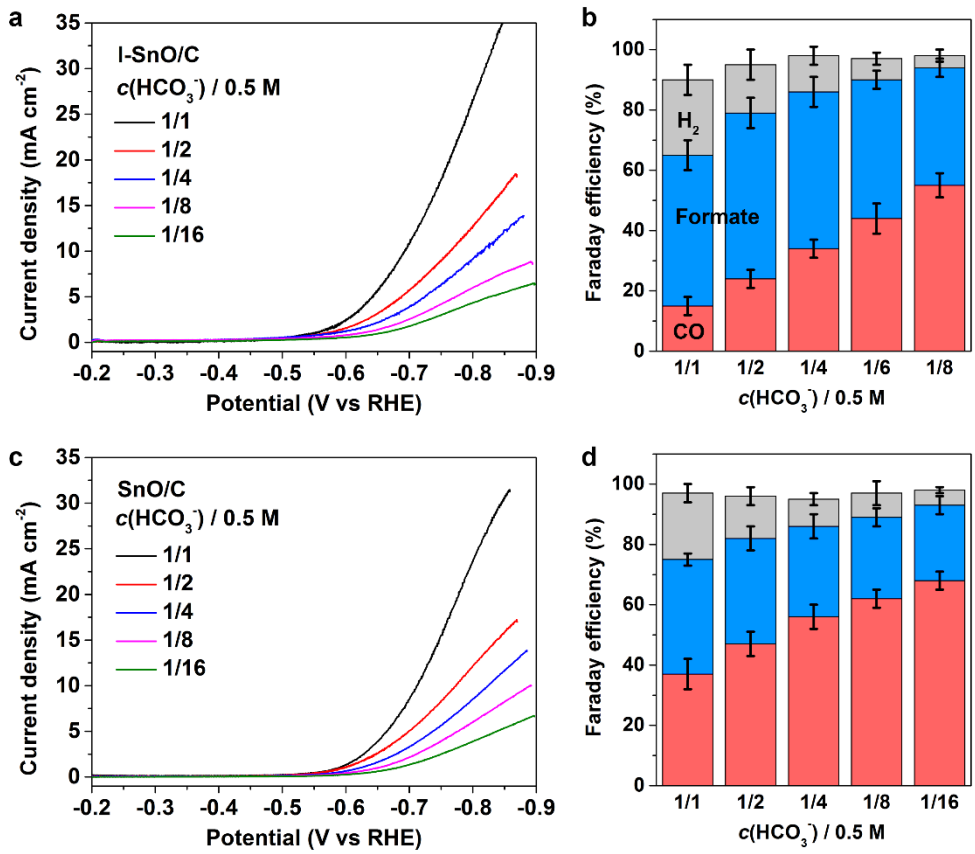

Figure S22. Stable LSV curves of l-SnO/C (a) and SnO/C (b) in CO_2 saturated $KHCO_3$-KCl electrolyte. The total concentration of $KHCO_3$ and KCl was 0.5 M and the concentration of $KHCO_3$ was 1/1 (black), 1/2 (red), 1/4 (blue), 1/8 (pink) and 1/16 (green) of 0.5 M. Faraday efficiency of CO (red), formate (blue) and H_2 (grey) of l-SnO/C (b) and SnO/C (d) at -0.66 V vs RHE in electrolytes with different concentration of $KHCO_3$. As the concentration of $KHCO_3$ in electrolyte decreased, the total current density decreased while the Faraday efficiency of CO increased.

Table S2. Fitting of Sn 3d XPS spectra of SnO/C, SnO_2/C and Sn/C.

Sample	Sn (0)		SnO		SnO_2	
	B.E. (eV)*	Fraction (%)	B.E. (eV)*	Fraction (%)	B.E. (eV)*	Fraction (%)
SnO/C	--	--	486.9	28	487.8	72
SnO_2/C	--	--	--	--	487.8	100
Sn/C	485.4	13	--	--	487.6	87

* Binding energy of Sn 3d5/2 peak.

Table S3. BET surface areas and BJH pore volumes of carbon black, Sn/C, SnO_2/C and SnO/C.

Sample	S_{BET} ($m^2 \cdot g^{-1}$)	V_p ($cm^3 \cdot g^{-1}$)
Carbon black	173	0.45
Sn/C	105	0.27
SnO_2/C	93	0.27
SnO/C	148	0.30

4. References

[1] S. Zhang, P. Kang, T. J. Meyer, *J. Am. Chem. Soc.* **2014,** *136*, 1734-1737.
[2] D. H. Won, C. H. Choi, J. Chung, M. W. Chung, E.-H. Kim, S. I. Woo, *ChemSusChem* **2015,** *8*, 3092-3098.
[3] F. Lei, W. Liu, Y. Sun, J. Xu, K. Liu, L. Liang, T. Yao, B. Pan, S. Wei, Y. Xie, *Nat. Commun.* **2016,** 7, 12697.
[4] F. Li, L. Chen, M. Xue, T. Williams, Y. Zhang, D. R. MacFarlane, J. Zhang, *Nano Energy* **2017,** *31*, 270-277.
[5] Y. Chen, M. W. Kanan, *J. Am. Chem. Soc.* **2012,** *134*, 1986-1989.
[6] W. Luc, C. Collins, S. Wang, H. Xin, K. He, Y. Kang, F. Jiao, *J. Am. Chem. Soc.* **2017,** *139*, 1885-1893.
[7] Q. Li, J. Fu, W. Zhu, Z. Chen, B. Shen, L. Wu, Z. Xi, T. Wang, G. Lu, J.-j. Zhu, S. Sun, *J. Am. Chem. Soc.* **2017,** *139*, 4290-4293.
[8] W. Cen, W. Wu, H. L. Ge, S. Tao, J. Z. Jiang, *Nanotechnology* **2012,** *23*, 075704.